2005

Comparative Analysis of Conventional and ICI-Self-Cancellation Digital Video Broadcasting Transceivers

Khaled Z. Matarneh
Louisiana State University and Agricultural and Mechanical College

COMPARATIVE ANALYSIS OF CONVENTIONAL AND ICI-SELF-CANCELLATION DIGITAL VIDEO BROADCASTING TRANSCEIVERS

A Thesis

Submitted to the Graduate Faculty of
the Louisiana State University and
Agricultural and Mechanical College
in partial fulfillment of the
requirements for the degree of
Master of Science in Electrical Engineering

in

The Department of Electrical and
Computer Engineering

by
Khaled Z. Matarneh
B.S.E.E, University of Arkansas, 2003
August 2005

ACKNOWLEDGMENTS

I would like to express my sincere thanks to Dr. Hsiao-Chun Wu, Chairman of my committee for his guidance and support throughout the course of this research. I am so grateful to him for giving me the opportunity to work on one of the fields he is involved in. I would also like to thank Dr. Subhash C. Kak, and Dr. Ashok Srivastava for their kindness and for being serving on my committee.

I would like to also thank Mr. Sameer Herlekar, a Ph. D. student who played a crucial role in guiding and helping me towards the completion of my thesis, for his precious time during the busy schedule for the beneficial discussions on my thesis work.

Last but not least, I would like to thank my parents, brothers, sister, my uncle Imad Matarneh, Abby Vinson, and all my friends for being there for me when I needed them and for believing in me no matter what. I owe all my success to all of those people. Without them I would not have made it this far.

TABLE OF CONTENTS

LIST OF ABBREVIATIONS

DVB: Digital Video Broadcasting

DVB-T: Digital Video Broadcasting-Terrestrial

DVB-H: Digital Video Broadcasting-Handhelds

OFDM: Orthogonal Frequency Division Multiplexing

ICI: Inter-Carrier Interference

ISI: Inter-Symbol Interference

PCC: Polynomial Cancellation Coder

SFN: Single Frequency Network

ABSTRACT

Digital video broadcasting–terrestrial (DVB-T) is one of the important technologies in the communication area because of its capability of high data-rate multimedia transmission. Orthogonal frequency division multiplexing (OFDM) has been the backbone technique in the current DVB-T systems adopted by Europe and Japan. However, since the OFDM system is very sensitive to the frequency synchronization and phase errors, which will induce the intercarrier interference (ICI), the ongoing research has been dedicated to this ICI problem in the presence of the Doppler frequency drift and the fading channels. A means to deal with the ICI problem is called the ICI self-cancellation or polynomial cancellation coding scheme. In this thesis, we establish the complete simulation environment for the physical layer of the DVB-T system and then evaluate the effectiveness of the ICI self-cancellation coding scheme compared with the existing convolutional coding scheme for different fading channels and different Doppler frequencies. According to our simulation results, we conclude that the ICI self-cancellation scheme significantly outperforms the convolutional coding scheme which is adopted by the existing DVB-T standard in the AWGN and the frequency non-selective fading channels, but both schemes have the similar performance in the frequency selective fading channels.

CHAPTER 1
INTRODUCTION OF DIGITAL VIDEO BROADCASTING (DVB)

Information transmission at higher data-rates with minimum error probability is one of the continuing research endeavors by the wireless communications researchers. For example, a recent research to achieve this goal is the digital video broadcasting (DVB) which was initiated in 1993. This DVB project is motivated to design a global standard for the broad-area delivery of digital terrestrial television and data services [1].

When the DVB service was first introduced, the two main pieces of displaying hardware were the TV receiver and the multimedia personal computer [1]. The DVB services were provided using cable, satellite, and terrestrial systems [1].

The main focus of this thesis is to analyze and simulate the digital video broadcasting-terrestrial (DVB-T) system, which is widely adopted in Europe and Japan. In chapter 1 we provide a brief introduction of the DVB-T system as well as the associated main features and discuss some aspects related to the performance of *mobile* DVB transceivers; we also introduce a new extension of the DVB family, namely the *digital video broadcasting-handhelds* (DVB-H), which is a modified version of the DVB-T system and can enhance the mobility support for the existing DVB-T systems. With such an enhanced capability, the DVB-H technology is expected to deliver different DVB services on handheld devices such as personal digital assistants (PDAs) and cellular phones [2]. However, the Doppler effect encountered by the mobile subscribers will induce the frequency-offset problem which leads to the intercarrier interference (ICI) and strictly limits the DVB quality-of-service [20, 22-24]. Since the current DVB-T or DVB-H standards are both based on the orthogonal frequency division multiplexing (OFDM)

technique [12, 28], the aforementioned problems can be combated with the help of the ICI self-cancellation coding scheme [20, 27]. However, the ICI self-cancellation or polynomial cancellation coding (PCC) scheme was just proposed for the plain OFDM system and has not been well tested for the DVB services. Therefore, we are motivated in this thesis to study the quality-of-service of the new DVB-T systems incorporated with the ICI self-cancellation or PCC coding in the presence of various system impairments caused by the channels, local oscillators and Doppler effect. In Chapter 2, we discuss the effects of two well-known system impairments in the DVB-T systems; namely, the *multipath fading* due to the wireless communication medium and the *Doppler effect* due to the mobile reception [3, 4]. In Chapter 3, we discuss the ICI effect, one of the crucial problems in the existing DVB-T systems, where all of the system impairments as stated in Chapter 2 are considered as the factors to cause the ICI. In Chapter 4, we present the ICI self-cancellation coding or PCC scheme to combat the ICI and analyze the corresponding performance margin over additive white Gaussian noise, frequency-non-selective and frequency-selective channels. Finally we provide the concluding remarks regarding our analysis and simulation results in Chapter 5.

1.1 Digital Video Broadcasting–Terrestrial (DVB-T) Systems

High-rate data transmission of multimedia can be achieved using cable networks (DVB-C) and satellite services (DVB-S) [1,5,6]. Recently, there was an increasing demand in the low-cost high data-rate multimedia transmission using terrestrial networks, and therefore the DVB-T system was born in 1996 [7].

Thereafter, terrestrial broadcasters were able to provide their services with much better reception quality. The DVB-T system is considered as the most complicated

system among all DVB systems, because it had to co-exist with other existing networks such as analog terrestrial television broadcasting systems with minimum interference between each other [1]. Also, terrestrial networks usually require higher operational efforts and maintenance costs compared to satellite and cable [8].

At the initial stages, the DVB-T system was basically targeted for stationary and portable multimedia reception [8, 9]. In recent years, the DVB services have been extended with mobility support for mobile subscribers. However, as noted earlier, in mobile communications, the multipath fading and the Doppler effect are the two phenomena which would cause the signal distortion at receivers. Consequently, the performance limitation of the DVB-T systems has been found when the mobile reception is considered [7, 8, 9].

To mitigate the effect of signal distortion, orthogonal frequency division multiplexing was adopted as the wireless-access technique for the DVB-T systems [8]. In OFDM-based systems, a serial data stream is transmitted in parallel on the multiple low-rate data substreams. Each substream of data is carried on a separate frequency, known as a *subcarrier*. Thus, the OFDM is capable of combating the multipath fading, where the transmitted signal is reflected off the objects such as buildings, foliage, vehicles, billboards, hillsides, and people and meanwhile, the duplicates of the transmitted signal arrive at the receiver at different times. This OFDM advantage makes possible the portable and mobile reception of the DVB-T signals [10].

From now on, we would like to study the transmission model for OFDM systems. During the signal transmission, the time difference between the earliest and the latest arriving signal duplicates is defined as the *multipath delay spread* [3]. When the

multipath delay spread is longer than the duration of the transmitted information symbol, *intersymbol interference* (ISI) occurs where the delayed duplicates of a previously transmitted symbol interfere with the current received symbol [10]. This usually results in a severe performance degradation in the conventional single-carrier communication systems [4]. However, in OFDM-based systems, this ISI problem can be considerably reduced by the inclusion of a guard interval or a cyclic prefix (a cyclic extension in time of the OFDM symbol) [10]. If the multipath delay spread is shorter than the guard interval, then no ISI takes place in OFDM systems [10].

The OFDM capability of mitigating the multipath fading effect leads to the plausibility of implementing the DVB-T systems on *single frequency networks* (SFNs) [10]. An SFN is a type of network where several base stations (transmitters) operate on the same carrier frequency and transmit identical data [1, 7, 10]. The use of SFNs leads to the advantages in frequency efficiency and broadcast coverage [10].

Figure 1 depicts the block diagram for the physical layer in an OFDM-based DVB-T system.

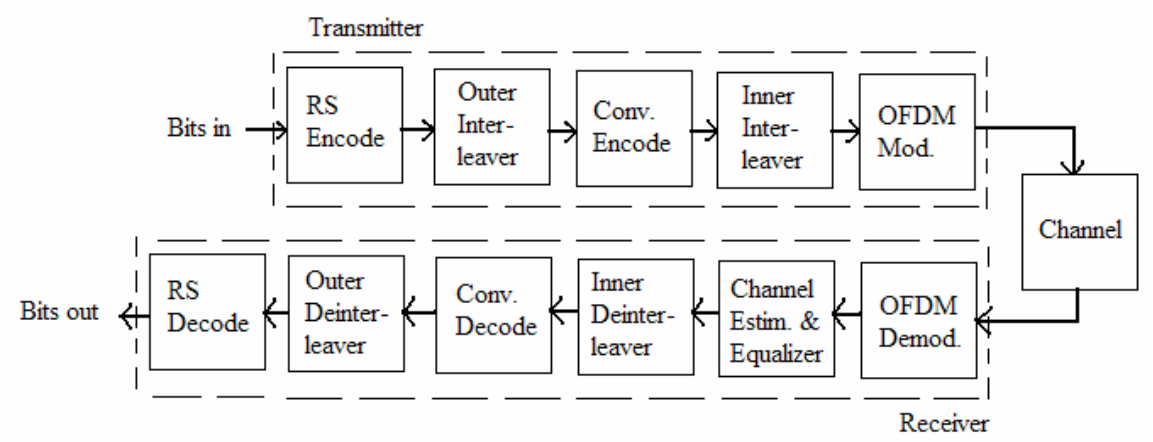

Figure 1. Physical layer of a DVB-T system.

According to the transmitter depicted in Figure 1, the existing error correction scheme used for the DVB-T system consists of a series of coding subsystems, where a Reed-Solomon (RS) block code is followed by a convolutional code (the two coders are then said to be *concatenated*) [9]. The purpose of the outer- and inner- interleavers is to spread the transmitted bit stream in time to prevent *burst errors* [7, 11], while the OFDM modulator allocates the interleaved bits onto the different subcarriers [7]. At the receiver, we have the similar set of modules to reverse the modulation operations in the transmitter except one additional module, namely the channel estimator and equalizer. Channel estimation is used to prepare the channel information for the equalizer in order to remove the channel distortion effect on the received DVB-T signals [11].

The DVB-T standard specifies two operational modes, namely, the 2k- and the 8k-modes. The 2k-mode employs 1,705 subcarriers in a 7.61 MHz bandwidth, while 8k-mode employs 6,817 subcarriers in the same bandwidth. Since the 2k-mode has a smaller number of subcarriers in the same bandwidth, the symbol duration for the 2k-mode is one fourth of the symbol duration for the 8k-mode. [11] That is why in a 2k-mode DVB-T system, the error-probability performance is four times better than that of the 8k-mode system against time-varying fadings [11]. However, due to the shorter symbol duration, the 2k-mode cannot be used effectively in multipath channels with long delays, which limit the usefulness of the 2k-mode for SFNs [11]. Hence, the 2k-mode is usually adopted for single transmitter operation or for small SFNs with a limited distance between transmitters [12]. The 8k-mode can be used for both single transmitter operation and large SFNs covering a broad area [12]. Table 1 lists some crucial parameters for both the 2k- and 8k-mode SFNs [2, 7, 9].

Table 1. Crucial DVB-T system parameters.

DVB-mode	2k	8k
Number of subcarriers	1705	6817
Carrier frequency	470-682 MHz	470-682 MHz
Symbol duration	224 μs	896 μs
Subcarrier spacing	4.464 kHz	1.116 kHz
OFDM bandwidth	7.61 MHz	7.61 MHz
Modulation	QPSK, 16-QAM, 64-QAM	QPSK, 16-QAM, 64-QAM
Code rate of inner convolutional coder	1/2, 2/3, 3/4, 5/6, 7/8	1/2, 2/3, 3/4, 5/6, 7/8
Guard interval duration	1/4: 56μs 1/8: 28μs 1/16: 14μs 1/32: 7μs	1/4: 224 μs 1/8: 112 μs 1/16: 56μs 1/32: 28μs
Maximum distance between transmitters (km)	17	67

It has been shown that the multimedia reception for both portable and mobile subscribers is possible using the DVB-T system, but only under certain restrictions. For example, if we use a receiver in a fast-moving vehicle, a DVB-T system would not always be reliable [1, 9]. In this thesis, an OFDM-based DVB-T system will be tested for different fading channels and for different frequency offsets through the computer simulations, where a comparison will be carried out between the system performances resulting from the two coding schemes; namely convolutional coding and ICI self-cancellation coding.

1.2 Digital Video Broadcasting – Handhelds (DVB-H) Systems

As mentioned in Section 1.1, the original DVB-T standards were targeted for the stationary reception. Lately, significant research endeavors were initiated to assess the feasibility of reliable mobile DVB-T systems. The existing research has shown that the reliability of the mobile DVB-T systems is not satisfactory [1, 7, 8, 9, 10, 11, 13]. Hence, the digital video broadcasting-handhelds (DVB-H) project was proposed as an alternative solution for mobile DVB-T systems [14]. The developments of the specifications regarding the DVB-H systems started in the fall of 2002, and the standard was finalized in February 2004 [2].

An uninterrupted and high-quality broadcast service is demanded for fast-moving vehicular reception. The DVB-H networks can serve this need by using *loss-free handover,* where a DVB-H receiver can switch among different frequencies without any loss of data [15]. In addition, the power consumption is a major concern for mobile subscribers. The *time slicing* operational mode is a unique feature brought by the DVB-H systems [2]. This new operational mode enables a DVB receiver to switch power off whenever no data is received. This time-slicing scheme reduces the power consumption of such receivers by 90% or more and leads to a longer battery life [2, 14]. This power-saving technique ensures a reasonable operating time for the battery-powered handsets.

Another advantage of using time slicing is that during the "*turn-off*" time, the mobile receiver can search for the channels with the same service in the neighboring radio cells [2, 14]. This results in a timely channel handover when the user is on the border of several cells. While the DVB-H receiver operates in the time slicing mode, the

data for a particular service is not transmitted continuously, but rather in compact periodical bursts with interruptions in between.

For the DVB-H systems, multiple services can be multiplexed into a continuous, uninterrupted data stream. Service multiplexing is performed in a pure time division multiplexing (TDM) scheme [2]. Figure 2 depicts this TDM scheme and also shows the service allocation difference between the DVB-T transmission and the DVB-H transmission with time slicing [2].

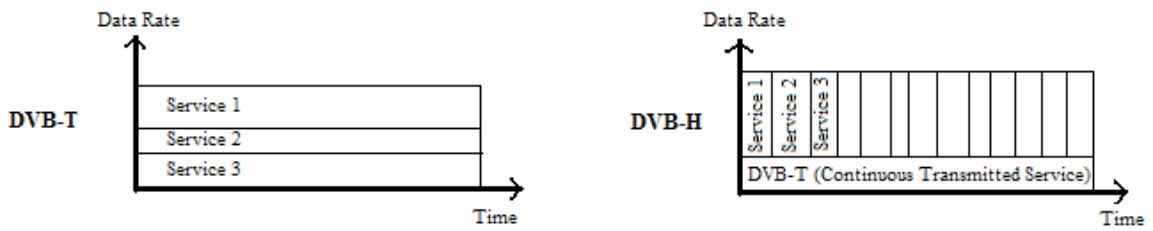

Figure 2. Service allocation difference between DVB-T and DVB-H.

DVB-H integrates an additional 4k-operational mode as a compromise solution between the two already-existing modes (2k- and 8k-modes) in the DVB-T systems [2]. Table 2 shows some crucial parameters among 2k-, 4k-, and 8k-modes [2].

Table 2. Comparison of the DVB-H system parameters for the new 4k-mode and the existing 2k- and 8k-modes.

Mode	2k	4k	8k
Number of subcarriers	1705	3409	6817
Symbol duration	224 µs	448 µs	896 µs
Subcarrier spacing	4.464 kHz	2.232 kHz	1.116 kHz
Guard interval duration	1/4: 56µs 1/8: 28µs 1/16: 14µs 1/32: 7µs	1/4: 112µs 1/8: 56µs 1/16: 28µs 1/32: 14µs	1/4: 224 µs 1/8: 112 µs 1/16: 56µs 1/32: 28µs
Maximum distance between transmitters (km)	17 km	33 km	67 km

According to Table 2, it is noted that the 4k-mode doubles the distance between transmitters (broadcasting base stations) in the SFNs compared to the 2k-mode. Furthermore, the 4k-mode is not as susceptible to the Doppler effect in mobile reception conditions as the 8k-mode. Hence, the new 4k-mode introduces more flexibility for network planning and management [2].

Another advantage of the DVB-H system is that it supports a 5 MHz bandwidth in addition to the three existing bandwidths supported by the DVB-T standard (6 MHz, 7 MHz, and 8 MHz). This will enable the usage of the DVB-H systems out of the typical broadcast frequency bands [2].

CHAPTER 2
CHANNEL MODELING FOR DIGITAL VIDEO BROADCASTING SYSTEMS

2.1 Fading Channels

After the transmitter broadcasts a signal, the signal propagates through the air to arrive at the receiver. During the propagation, the signal encounters the objects such as hills, forests, billboards, and even ions in the ionospheric layers that all affect the signal in many different ways. Three major phenomena including the signal's reflection, diffraction, and scattering arise [16]. We would like to focus on the reflection phenomenon and the *multipath propagation* here in this thesis. However, we will provide a brief discussion about how the two other mechanisms affect the signal propagation as well.

In diffraction, when a signal runs into an object, the object gives rise to the secondary waves that are formed behind the object and distort the subject signal [16]. In scattering, the obstacles in the signal propagation path make the subject signal scattered in many directions and lead to the signal energy attenuation [16].

Reflection occurs when the propagating signal impinges on an object with a smooth surface which has very large dimensions compared to the signal's wavelength [16]. As illustrated in Figure 3, the received signal is composed of the signal received from the *direct path* as well as those received from the *secondary paths* between the transmitter and the receiver. This process is termed *multipath propagation* of the transmitted signal [4].

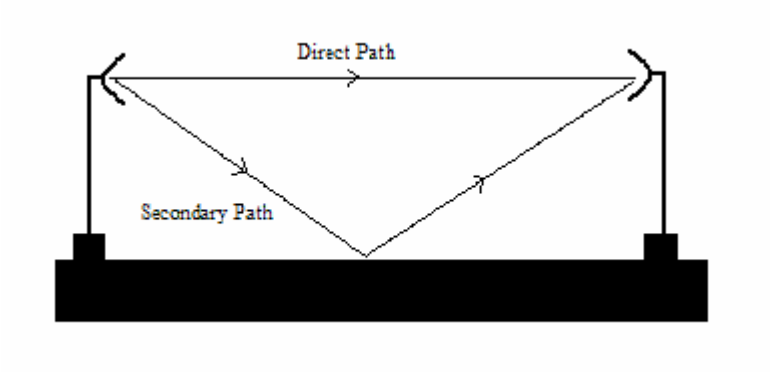

Figure 3. Illustration of multipath propagation (two-path).

In order to model the multipath propagation effect as previously described, we make use of the basic communication transceiver model depicted in Figure 4. As illustrated in Figure 4, the transmitted *baseband signal* $b(t)$ is converted to a radio-frequency (RF) signal $x(t)$ using a frequency up-converter. Such a signal $x(t)$ is then transmitted into the RF channel; the arriving signal $r(t)$ at the receiver is then converted back into a baseband signal $y(t)$ via a frequency down-converter.

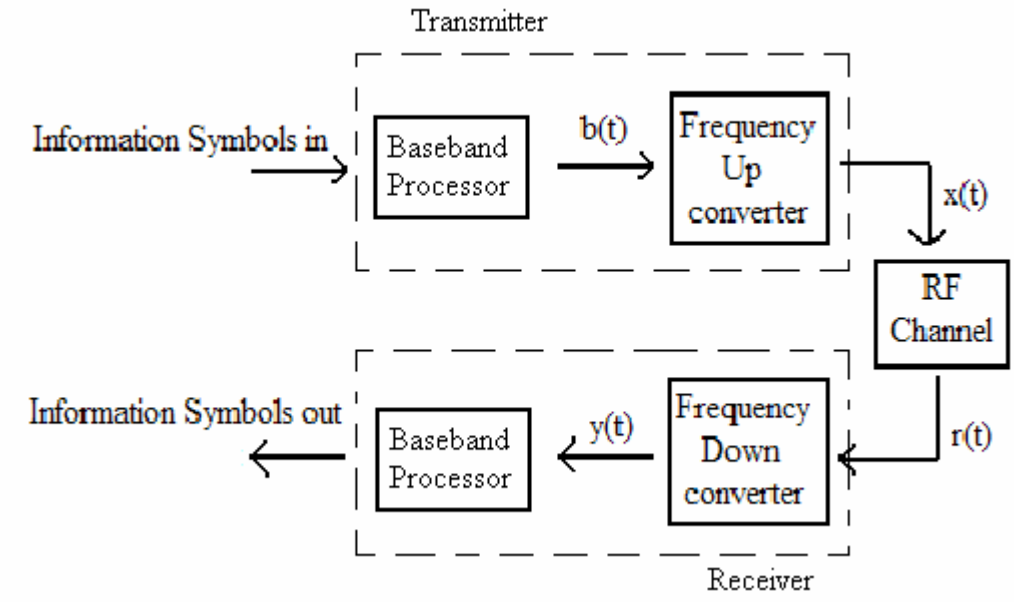

Figure 4. Basic communication transceiver model.

According to Figure 4, the transmitted RF signal $x(t)$ can be expressed as [3]:

$$x(t) = \mathrm{Re}\{b(t)\exp(j2\pi f_c t)\}, \tag{1}$$

where f_c is the carrier frequency. The received signal $r(t)$ can be formulated as [3]:

$$r(t) = \sum_{p=1}^{M} \alpha_p(t)\, x(t-\tau_p(t)), \tag{2}$$

where $\alpha_p(t)$ and $\tau_p(t)$ are the time-varying channel gain and the time-varying propagation delay corresponding to the p^{th} propagation path respectively, $x(t)$ is the transmitted signal given by Eq. (1), and M is the total number of received signal components or the number of propagation paths. According to Eqs. (1) and (2), the baseband signal y(t) can be derived as

$$\begin{aligned} y(t) &= \sum_{p=1}^{M} \alpha_p(t)\exp\left(-j2\pi f_c \tau_p(t)\right) b\left(t-\tau_p(t)\right) \\ &= \sum_{p=1}^{M} \alpha_p(t)\exp\left(-j\theta_p(t)\right) b\left(t-\tau_p(t)\right), \end{aligned} \tag{3}$$

where $\theta_p(t) = 2\pi f_c \tau_p(t)$.

According to Eq. (3), $y(t)$ comprises a sum of multiple copies of the transmitted signal $b(t)$ with respective time-varying amplitudes $\alpha_p(t)$ and respective time-varying propagation delays $\tau_p(t)$ [3]. At the receiver, those signal duplicates interfere with each other constructively or destructively and result in the amplification or attenuation of $y(t)$. Such received signal amplitude fluctuations are called *multipath fading* [3].

In practical mobile communication systems, the multipath fadings can be categorized as *large-scale fading* and *small-scale fading* [16, 19]. Large-scale fading arises from a large-displacement motion (in the order of tens or hundreds of meters) and

leads to signal power attenuation, or *path loss* [4,16]. On the other hand, small-scale fading manifests a rapid fluctuation in both signal amplitude and phase which arises from the small changes (in the order of a half-wavelength of the transmitted signal) in the distance between the transmitter and the receiver [16, 19]. Figure 5 provides an overview of the different fading manifestations induced by wireless channels [16].

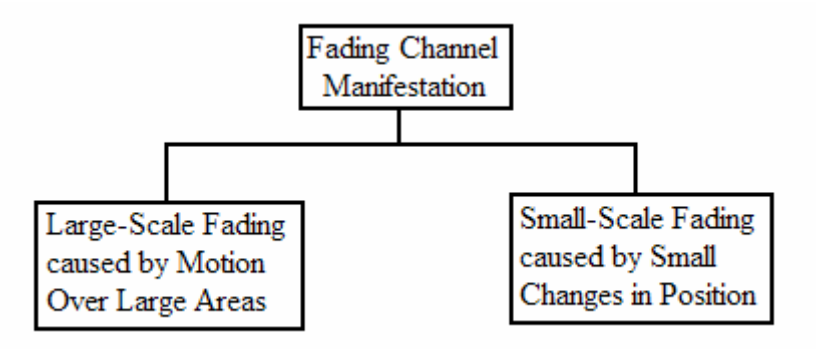

Figure 5. Channel fading characterization.

In this thesis, our main focus will be on the small-scale fading to model the channel characteristics for digital video broadcasting systems. The small-scale fading manifests itself in two ways, by the *time-spreading* of the transmitted signal, and by the *time-varying* behavior of the channel [16]. The time-spreading effect is discussed in more detail in Section 2.2 of this thesis while the *time-varying* nature of the channel is described in Section 2.3.

2.2 Time-spreading Effect of the Multipath Propagation

When we transmit a signal into a multipath channel, the received signal generally appears as a combination of signals with time-varying amplitudes, time-varying phases and random interarrival times [3, 4] . This is called the *time spreading* effect of the

multipath propagation and it is depicted in Figure 6. According to Figure 6, the transmitted signal approximates the Dirac-delta function, defined as [29]:

$$\delta(t-\tau_0)=\begin{cases}\infty & ,t=\tau_0\\ 0 & ,t\neq\tau_0\end{cases} \tag{4}$$

and $$\int_{-\infty}^{+\infty}\delta(t-\tau_0)\,dt=\int_{\tau_0-}^{\tau_0+}\delta(t-\tau_0)dt=1\,. \tag{5}$$

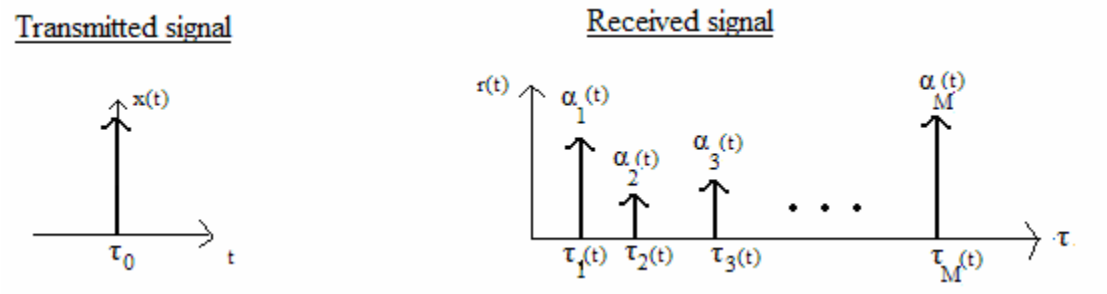

Figure 6. Time-spreading effect of the multipath propagation.

According to Eq. (2) and Figure 6, it is noted that at a given observation time *t*, the received signal $r(t)$ is composed of *M* signals with random amplitudes $\{\alpha_p(t)\}_{1\le p\le M}$ and random arrival times $\{\tau_p(t)\}_{1\le p\le M}$. The arrival-time difference between the first and the last received signal copies is called the *maximum excess delay* $T_m(t)$ associated with the channel, or, $T_m(t)\overset{\Delta}{=}\tau_M(t)-\tau_1(t)$ [16]. For notational convenience, we usually set $\tau_1(t)=0$ [4].

The time-spreading effect as illustrated in Figure 6 induces two types of fadings, namely *frequency-selective* fading and *frequency-nonselective* fading [16, 19]. Frequency-selective fading occurs when the maximum excess delay $T_m(t)$ is larger than

the information symbol duration T_S, i.e., $T_m(t) > T_S$ [16]. This type of fading causes the received signal copies to overlap with each other and results in the *inter-symbol interference* (ISI), as well as the deterioration of system performance [3, 4, 16]. On the other hand, frequency-nonselective fading occurs if $T_m(t) < T_S$ [16]. In this case, all the received multipath components of a transmitted signal arrive within one symbol duration T_S. Frequency-nonselective fading does not result in ISI; nevertheless, as mentioned in Section 2.1, the received multipath components may still interfere with each other destructively and lead to the system performance degradation [16, 19]**.**

An analogous characterization of the time spreading effect can be made in the frequency domain, in terms of *channel coherence bandwidth* [3, 4, 16]. The *coherence bandwidth* f_0 is a statistical measure of the frequency range within which the channel passes all the frequency components with nearly equal gain and linear phase [4]. A channel is said to be frequency-selective if $f_0 < W$, where $W = 1/T_S$ approximates the signal bandwidth [3, 4, 16]. The signal's frequency components beyond the coherence bandwidth experience different gains from those within the coherence bandwidth [4]. On the other hand, frequency non-selective fading occurs when $f_0 > W$, where all of the signal's frequency components experience a very similar fading effect due to the channel [16]. However, it is noted that the condition $f_0 > W$ does not guarantee that the channel will always be frequency non-selective [16]. For example, a mobile receiver can experience frequency-selective distortion even if the condition $f_0 > W$ exists because the additional Doppler effect is also considered therein [16]**.**

In summary, Figure 7 categorizes the small-scale fadings due to the multipath propagation [16, 19].

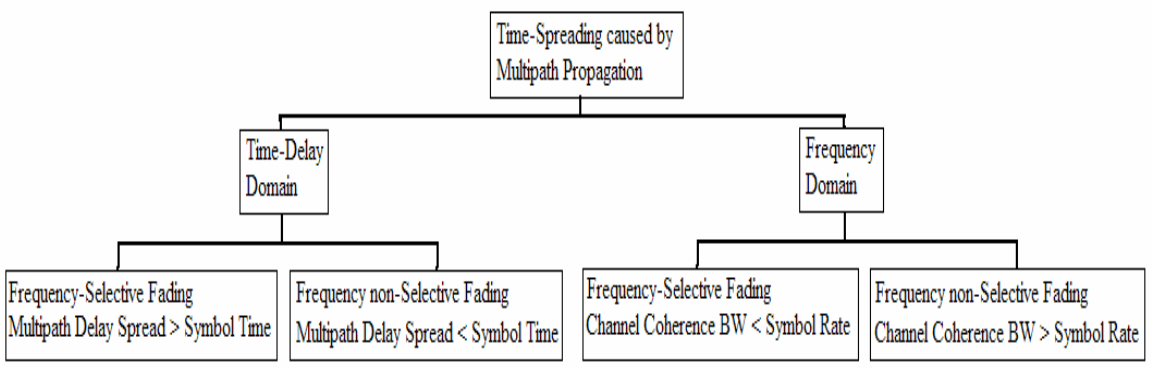

Figure 7. Categorization of small-scale fadings due to the time-spreading mechanism.

2.3 Doppler Effect due to the Mobility

In this section, we study the effect of the channel's time-varying nature. Consider a receiver in a vehicle that is moving in a distance *d* between points *X* and *Y* at a constant velocity *v*, while receiving a signal from a remote transmitter *S*, as illustrated in Figure 8 [4].

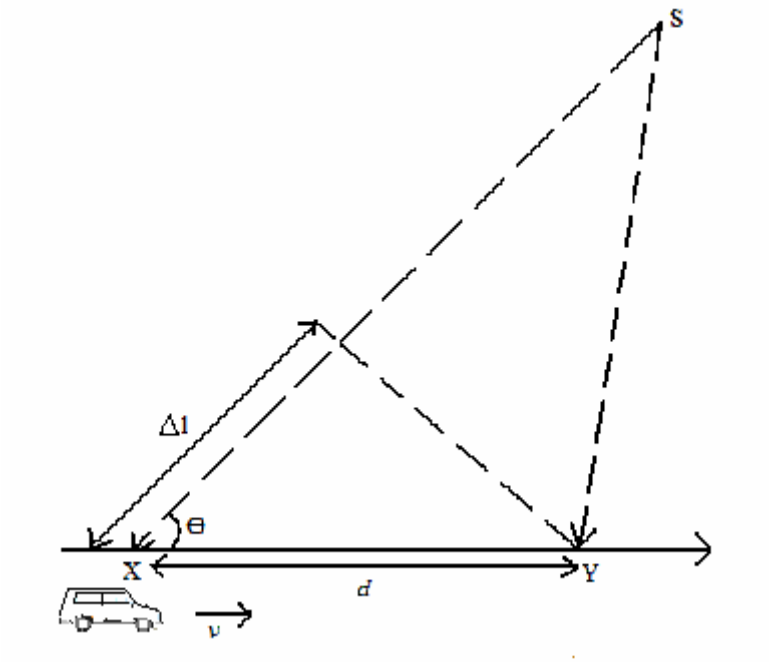

Figure 8. Illustration of the Doppler effect.

According to Figure 8, the difference between the path lengths traveled by the signal from the distant source *S* to the mobile terminals at points *X* and *Y* is $\Delta l = d\cos\theta = v\,\Delta t\cos\theta$, where Δt is the time for the vehicle to travel from point *X* to point *Y*, and θ is the angle between the vehicle's moving direction and the path between the transmitter and receiver at a given time [4]. The *phase change* in the received signal due to the difference in path lengths is given by [4]

$$\Delta\phi = \frac{2\pi\,\Delta l}{\lambda} = \frac{2\pi\, v\Delta t\cos\theta}{\lambda}, \tag{6}$$

where λ is the wavelength of the transmitted RF signal. The phase change $\Delta\phi$ leads to an apparent change f_d in the received signal's frequency, such that [4]:

$$f_d = \frac{1}{2\pi}\frac{\Delta\phi}{\Delta t} = \frac{v}{\lambda}\cos\theta\,. \tag{7}$$

Such a frequency change f_d is also known as the *Doppler shift* in the literature [4, 16]. According to Eq. (7), it is noted that when $\theta = 0°$, we obtain $(f_d)_{\max} = f_m = v/\lambda$ and when $\theta = 90°$, $f_d = 0$.

Consequently, when a signal is transmitted at carrier frequency f_c, the received signal contains the spectral components between $f_c - f_d$ and $f_c + f_d$. This phenomenon is also known as *spectral broadening* [4,16]. The maximum spectral broadening results when $f_d = f_m$, which is called *Doppler spread* and it is illustrated in Figure 9.

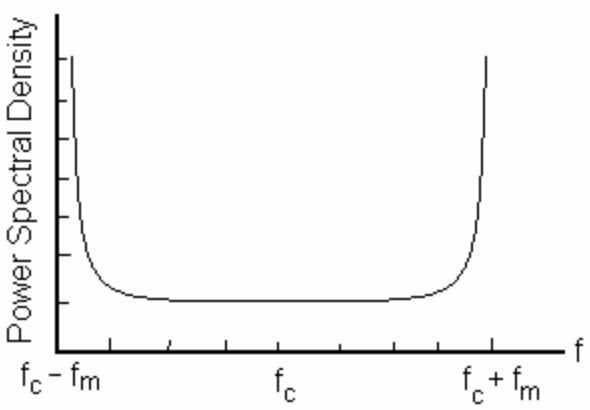

Figure 9. Doppler spread effect in the presence of maximum spectral spreading.

The Doppler spread f_m can be considered as a statistical measure of the *fading rate*, which indicates how fast the fading characteristics change [16].

Based on the fading rate, a multipath fading channel can also be classified as either a *fast fading* channel or a *slow fading* channel [4]. A channel is considered fast fading if $f_m > W = 1/T_s$ [3, 4, 16]. In other words, the fading characteristics of the channel change during the transmission of one OFDM symbol [16]. This type of fading causes the signal distortion and the degradation in OFDM system performance. On the other hand, slow fading occurs when $f_m < W$ [3, 4, 16]. In this case, the fading characteristics of the channel remain essentially stationary during the transmission of one OFDM symbol [16]. The impact of the slow fading channel on the OFDM system performance will be relatively less severe than that of the fast fading channel [16].

In the time domain, fast fading occurs when $T_s > T_0$, where T_0 is the *channel coherence time* and T_s is the symbol duration [4]. The channel coherence time T_0 is the time duration in which the channel's fading characteristics remain essentially stationary

[16]. If $T_s < T_0$, the channel is slow fading [4]. In summary, we provide Figure 10 to categorize the small-scale fadings, which are caused by the mobile reception [16, 19].

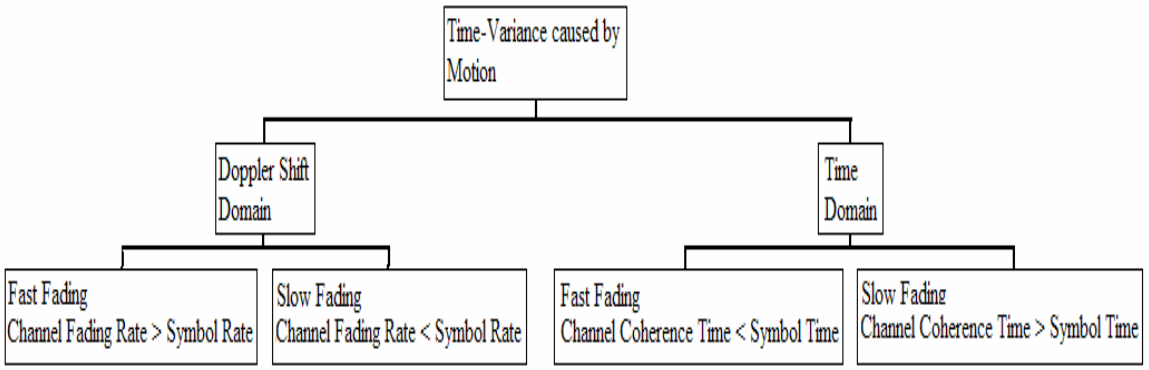

Figure 10. Categorization of small-scale fading due to time variance or mobile reception.

The aforementioned Doppler spread introduces the intercarrier interference (ICI) between the OFDM subcarriers and leads to the degradation of the OFDM system performance [30]. The impact of the ICI on the OFDM system performance will be analyzed in detail in Chapter 3.

CHAPTER 3
INTERCARRIER INTERFERENCE IN DIGITAL VIDEO BROADCASTING

3.1 Introduction of Intercarrier Interference in OFDM

Although the OFDM systems have the advantage in the frequency-selective fading channels, they are still sensitive to any frequency offset due to the Doppler spread or synchronization error in local oscillators [20, 23, 24] . Such frequency offsets will result in the intercarrier interference (ICI) and a rotation and an attenuation of each OFDM subcarrier signal [20-23]. To analyze this ICI problem, we provide the figure below to illustrate an OFDM system diagram [20].

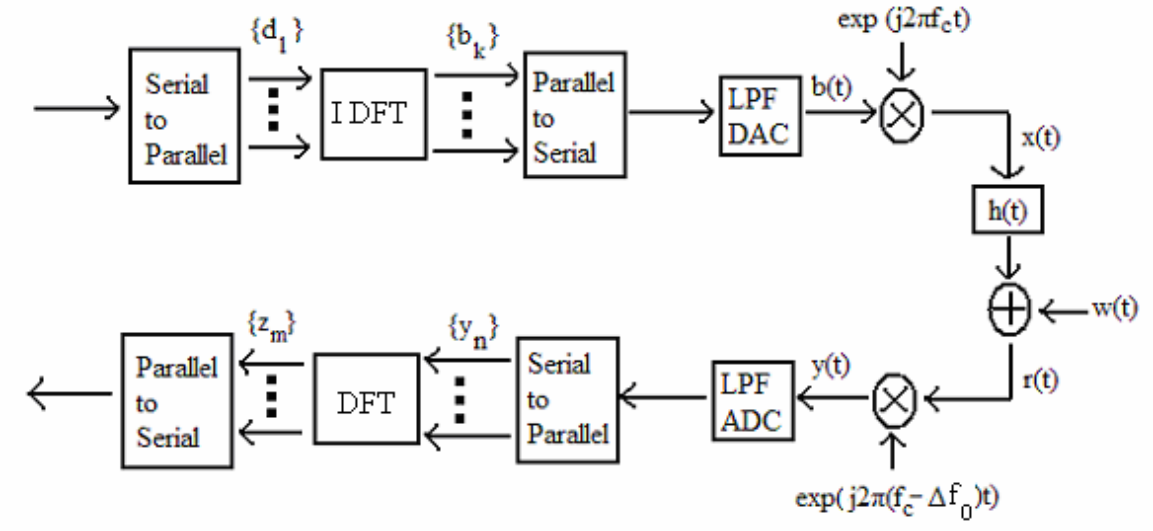

Figure 11. OFDM modulation and demodulation block diagram.

According to Figure 11, the information symbols are separated into N subcarriers, and $\{d_l\}_{0\le l\le N-1}$ denotes the corresponding $N\times 1$ signal vector in an OFDM block. Then we send $\{d_l\}_{0\le l\le N-1}$ through the inverse discrete Fourier transform (IDFT) and the output can be written as [20]:

$$b_k = \frac{1}{N}\sum_{l=0}^{N-1} d_l \exp\left(\frac{j2\pi lk}{N}\right),\ 0 \le k \le N-1. \tag{8}$$

The complex-valued symbol stream $\{b_k\}_{0\le k\le N-1}$ is fed into a lowpass filter (LPF) and a digital-to-analog converter (DAC) which produce the baseband OFDM signal $b(t)$ given by

$$b(t) = \frac{1}{N}\sum_{l=0}^{N-1} d_l \exp\left(\frac{j2\pi lt}{T}\right), \tag{9}$$

where T is the symbol period in seconds. The baseband signal $b(t)$ can be modulated at the carrier frequency f_c such that

$$x(t) = \mathrm{Re}\{\exp(j2\pi f_c t)\, b(t)\}. \tag{10}$$

$x(t)$ is the transmitted radio-frequency signal to the channel. At the receiver, the arriving signal can be modeled as

$$r(t) = x(t) \otimes h(t) + w(t), \tag{11}$$

where $h(t)$ is the channel impulse response, and $w(t)$ is the additive white Gaussian noise (AWGN). Disregarding $w(t)$, the received signal $r(t)$ can be formulated as [30]:

$$\begin{aligned} r(t) &= \sum_{p=1}^{M} g_p(t)\, x\left[t-\tau_p(t)\right] \quad , \\ &= \mathrm{Re}\Big\{\exp(j2\pi f_c t)\cdot \\ &\qquad \sum_{p=1}^{M} g_p(t)\exp\left(-j2\pi\left(f_c+\Delta f_p\right)\tau_p(t)\right)\cdot\exp(j2\pi\Delta f_p t)\, b[t-\tau_p(t)]\Big\} \end{aligned} \quad , \tag{12}$$

where $g_p(t)$ is the channel attenuation factor associated with the p^{th} path, $\tau_p(t)$ is the propagation delay of the p^{th} path and Δf_p is the Doppler shift corresponding to the p^{th} path. According to Figure 11, the down-carried signal can be obtained as

$$y(t) = \frac{1}{N} \exp(j2\pi\Delta f_o t) \cdot \sum_{p=1}^{M} g_p(t) \exp\left(j\theta_p(t)\right) \exp\left(j\psi_p(t)\right) \sum_{l=0}^{N-1} d_l \exp\left(\frac{j2\pi l\left[t-\tau_p(t)\right]}{T}\right), \quad (13)$$

where $\theta_p(t) = -2\pi\left(f_c + \Delta f_p\right)\tau_p(t)$, and $\psi_p(t) = -2\pi\Delta f_p t$, Δf_p is the Doppler frequency of the p^{th} path, Δf_o is the frequency offset resulting from the synchronization error in the receiver local oscillator [30]. Eq. (13) provides the formulation of the OFDM transmission model for the frequency selective fading.

We assume that $\tau_p(t) = \tau_p$, $\forall t$, [18]. Then, according to Figure 11, the sampled baseband OFDM signal y_n can be written as

$$y_n = \frac{1}{N} \exp\left(\frac{j2\pi n\Delta f_0 T}{N}\right) \sum_{p=1}^{M} g_p(nT_s) \exp\left(-j2\pi\left(f_c + \Delta f_p\right)\tau_p\right) \cdot \exp\left(\frac{j2\pi\Delta f_p nT}{N}\right) \sum_{l=0}^{N-1} d_l \exp\left(\frac{j2\pi ln}{N}\right) \cdot \exp\left(\frac{-j2\pi l\tau_p}{T}\right), \quad 0 \le n \le N-1, \quad (14)$$

The demodulated OFDM signal sequence after the discrete Fourier transform (DFT) can be written as

$$z_m = \sum_{n=0}^{N-1} y_n \exp\left(\frac{-j2\pi nm}{N}\right), \quad 0 \le m \le N-1. \quad (15)$$

Substituting Eq.(14) into Eq. (15), we obtain

$$z_m = \frac{1}{N} \sum_{p=1}^{M} \exp\left(-j2\pi\left(f_c + \Delta f_p\right)\tau_p\right) \cdot \sum_{n=0}^{N-1} g_p(nT_s) \sum_{l=0}^{N-1} d_l \exp\left(\frac{j2\pi n(l-m+\Delta f_o T - \Delta f_p T)}{N}\right) \exp\left(-\frac{j2\pi l\tau_p}{T}\right) \quad (16)$$

Alternatively, such a sequence z_m can also be written as [20]:

$$z_m = \sum_{l=0}^{N-1} c_{l-m}\, d_l, \tag{17}$$

where

$$c_{l-m} = \frac{1}{N}\sum_{p=1}^{M} \exp\left(-j2\pi\left(f_c + \Delta f_p\right)\tau_p\right)\cdot \sum_{n=0}^{N-1} g_p(nT_s)\exp\left(\frac{j2\pi n(l-m+\Delta f_o T - \Delta f_p T)}{N}\right)\exp\left(-\frac{j2\pi l\tau_p}{T}\right)$$

(Frequency selective model) (18)

To model the effect of a frequency non-selective Rayleigh fading channel, we can approximate the channel impulse response as a Dirac-delta function whose amplitude varies according to a Rayleigh distribution [4]. Therefore, according to Eq. (13), we can express the signal received from a frequency non-selective fading channel by setting M = 1 and $\tau_p(t) = 0$, $\forall p$ [4]. According to Figure 11 and Eq. (14), the sampled baseband OFDM signal y_n can then be written as

$$y_n = \frac{1}{N}\exp(\frac{j2\pi n\Delta f_0 T}{N})\, g(n)\exp\left(j\psi_1(nT_S)\right)\sum_{l=0}^{N-1} d_l \exp(j\frac{2\pi ln}{N}),\ 0 \le n \le N-1, \tag{19}$$

where $g(n)$ is the channel attenuation factor and $\psi_1(nT_s) = -2\pi\Delta f_1 nT_s$, $0 \le n \le N-1$ [30].

The demodulated OFDM signal sequence after the discrete Fourier transform (DFT) can be written as

$$z_m = \sum_{n=0}^{N-1} y_n \exp\left(\frac{-j2\pi nm}{N}\right),\ 0 \le m \le N-1. \tag{20}$$

Substituting Eq.(19) into Eq. (20), we obtain

$$z_m = \frac{1}{N}\sum_{l=0}^{N-1} d_l \sum_{n=0}^{N-1} g(n)\exp\left(\frac{j2\pi n(l-m+\Delta f_0 T+\Delta f_1 T)}{N}\right),\ 0 \le m \le N-1. \quad (21)$$

It can be seen from Eq. (21) that if $\Delta f_1 = 0$ and $g(n) = 1,\ \forall n$, the channel can be simplified as the well-known AWGN channel, where the demodulated OFDM sequence can be further simplified as [20]:

$$z_m = \frac{1}{N}\sum_{l=0}^{N-1} d_l \sum_{n=0}^{N-1} \exp\left(\frac{j2\pi n(l-m+\Delta f_o T)}{N}\right),\ 0 \le m \le N-1. \quad (22)$$

Alternatively, such a sequence z_m can also be written as [20]:

$$z_m = \sum_{l=0}^{N-1} c_{l-m}\, d_l, \quad (23)$$

where

$$c_{l-m} = \frac{1}{N}\sum_{n=0}^{N-1} \exp\left(\frac{j2\pi n(l-m+\Delta f_0 T)}{N}\right),\ 0 \le m,l \le N-1.$$

(AWGN model) (24)

It can be derived that [20]:

$$c_{m'} = c_{l-m},$$

where m' is an integer $(l-m)$ modulo N. Thus, Eq.(23) can then be written as

$$z_m = d_m c_0 + e_m,\ 0 \le m \le N-1, \quad (25)$$

where the ICI sequence e_m is defined as

$$e_m \overset{\Delta}{=} \sum_{l=0, l\neq m}^{N-1} c_{m'} d_l \ . \quad (26)$$

Eq. (25) shows that z_m consists of a subject information symbol d_m which has been attenuated and phase-rotated by the weighting coefficient c_0 in the presence of ICI e_m, which is a linear combination of other information symbols d_l, $\forall l \neq m$. According to Eq. (21) with $\Delta f_0 = 0$, the demodulated OFDM signal z_m can be reformulated as

$$z_m = \frac{1}{N} \sum_{l=0}^{N-1} d_l \sum_{n=0}^{N-1} g(n) \exp\left(\frac{j2\pi n(l-m+\Delta f_1 T)}{N} \right), \; 0 \le m,l \le N-1. \tag{27}$$

Eq. (27) provides the formulation of OFDM transmission model for a frequency non-selective channel, where the ICI is solely induced by the Doppler shift Δf_1 experienced by the received signal $r(t)$ as given by Eq. (12). In this case, z_m can be written as [20]:

$$z_m = \sum_{l=0}^{N-1} c_{l-m} \, d_l \; , \; 0 \le m,l \le N-1, \tag{28}$$

where

$$c_{l-m} = \frac{1}{N} \sum_{n=0}^{N-1} g(n) \exp\left(\frac{j2\pi n(l-m+\Delta f_1 T)}{N} \right), \; 0 \le m,l \le N-1.$$

(Frequency non-selective model) (29)

3.2 OFDM Performance Degradation due to Intercarrier Interference

According to Eq. (25) in Section 3.1, the demodulated OFDM sequence consists of the subject information symbol and an ICI term. It is noted that the higher the local oscillator frequency offset Δf_o, the lower the power of the subject information symbol $c_0 d_m$ and the more the power of the ICI e_m [27], for subcarrier m, $0 \le m \le N-1$.

The power of the subject signal for the m^{th} demodulated subcarrier can be written as [27]: $E\left[\left|c_0 d_m\right|^2\right]$, where E is the statistical expectation operator. The ICI effect can be quantified as the *ICI power*, which is defined as

$$E\left[\left|e_m\right|^2\right] \stackrel{\Delta}{=} E\left[\left|\sum_{l=0, l\neq m}^{N-1} d_l\, c_{l-m}\right|^2\right]. \tag{30}$$

The overall impact of the ICI on the OFDM system performance can be evaluated in terms of carrier-to-interference ratio (CIR) [23]. The information symbols $\{d_m\}_{0\le m\le N-1}$ are assumed to have zero mean and be statistically independent, such that the CIR for the m^{th} subcarrier can be derived as [23, 27]:

$$CIR = \frac{\left|c_m\right|^2}{\sum_{l=0, l\neq m}^{N-1}\left|c_{l-m}\right|^2} = \frac{\left|c_0\right|^2}{\sum_{l=1}^{N-1}\left|c_l\right|^2}. \tag{31}$$

In the AWGN channels, the carrier-to-interference ratio will only depend on the normalized frequency offset $\Delta f_o T$, according to Eqs. (24) and (31). The carrier-to-interference ratio for the frequency non-selective fading channels would depend on the normalized Doppler frequency offset $\Delta f_1 T$ and the channel gain $g(n)$, according to Eq. (29).

Generally speaking, the windowing of the transmitted signal in [25, 26], and the ICI self-cancellation coding in [27] are the two primary methods proposed to mitigate the ICI for the wireless OFDM systems. In this thesis, we focus on the ICI self-cancellation coding scheme to combat the ICI problem which has been induced by the receiver synchronization errors, the Doppler effect and the multipath propagation as discussed in this chapter.

CHAPTER 4
ICI SELF-CANCELLATION RECEIVERS FOR DIGITAL VIDEO BROADCASTING

4.1 ICI Self-Cancellation Receivers

Recently, a simple method to mitigate the effect of the frequency errors arising in OFDM was introduced and it was called ICI self-cancellation scheme [20,27]. In the OFDM transceiver with the ICI self-cancellation scheme, the information symbols d_l drawn from an M-QAM signal constellation are mapped onto adjacent pairs of subcarriers in the i^{th} OFDM block such that $d_{0,i} = -d_{1,i}$, $d_{2,i} = -d_{3,i}$, …, $d_{N-2,i} = -d_{N-1,i}$ [20, 27]. Thus, the resulting demodulated sequence $z_{0,i}$, …, $z_{N-1,i}$ in the i^{th} OFDM block can be modeled as

$$z_{m,i} = \sum_{l=0}^{N-1} c_{l-m}\, d_{l,i}\,,\ m = 0,1,2,....N-1\,, \tag{32}$$

where c_{l-m} are the ICI weighting coefficients as described by Eqs. (18), (24), and (29) in Chapter 3. For example, the demodulated OFDM sample for the zeroth subcarrier is given by [20]:

$$z_{0,i} = (c_0 - c_1)d_{0,i} + (c_2 - c_3)d_{2,i} + ... + (c_{N-2} - c_{N-1})d_{N-2,i}\,. \tag{33}$$

According to Eq. (24) for an AWGN channel, the ICI would be greatly mitigated and the resulting carrier-to-interference ratio (CIR) can be quantified as [27]:

$$CIR \overset{\Delta}{=} \frac{\left|-c_{-1} + 2c_0 - c_1\right|^2}{\sum_{l=2,4,6,...}^{N-1} \left|-c_{l-1} + 2c_l - c_{l+1}\right|^2}\,. \tag{34}$$

According to Eq. (34), this ICI self-cancellation scheme greatly enhances the carrier-to-interference ratio, which is the primary objective measure for the OFDM quality-of-service, especially for mobile subscribers in the fading channels [17].

4.2 DVB Performance Evaluation Using ICI Self-Cancellation or PCC Scheme

The existing literature provides only primitive analyses regarding the ICI self-cancellation or PCC scheme for a plain OFDM system where all of other major features such as channel coders and interleavers are absent [20, 27, 17]. Since most of wireless standards, including the DVB-T and the DVB-H, comprise those sophisticated features [12, 28], the ICI self-cancellation or PCC scheme has not been tested for the complete OFDM system complying with any wireless standard yet. Besides, the performance of the ICI self-cancellation OFDM receivers has not been studied in terms of different fading environments either. In this thesis, we would like to provide the new analysis for the ICI self-cancellation OFDM transceivers regarding the digital video broadcasting applications. To serve this purpose, a complete OFDM-based DVB-T system was implemented as depicted in Figures 12 and 13.

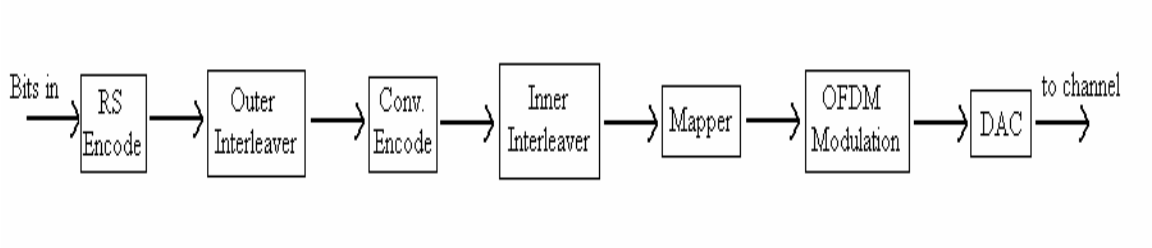

Figure 12. OFDM-based DVB-T transmitter.

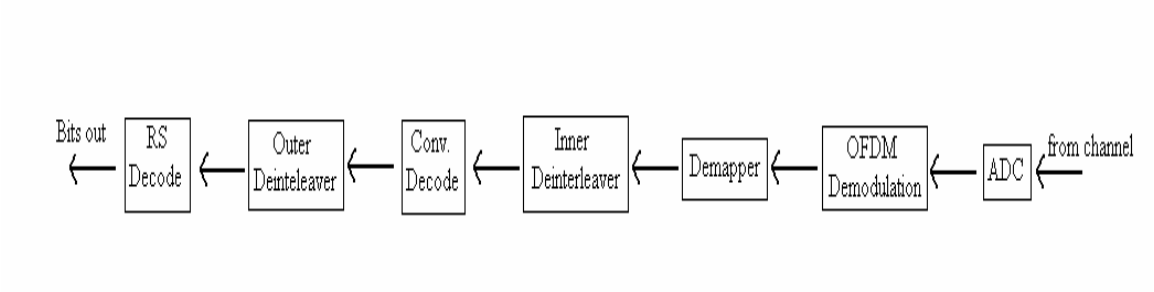

Figure 13. OFDM-based DVB-T receiver.

With the identical spectral efficiency, the convolutional coder can be replaced by the ICI self-cancellation coder in a DVB-T system as shown in Figures 14 and 15.

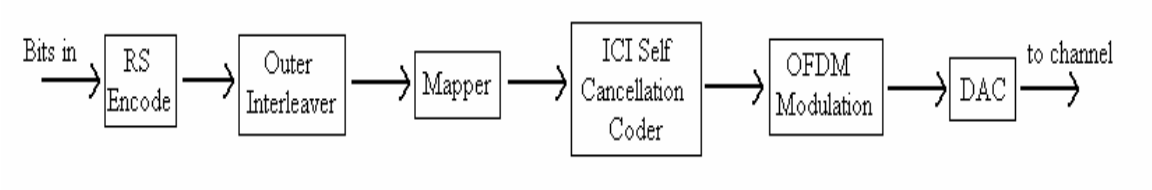

Figure 14. ICI self-cancellation DVB-T transmitter.

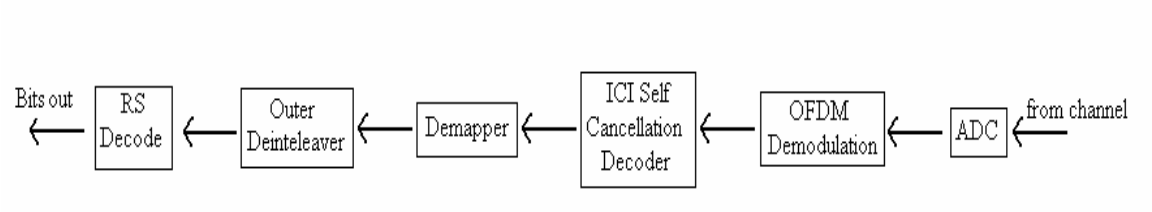

Figure 15. ICI self-cancellation DVB-T receiver.

We compare two different DVB-T systems here, namely the existing DVB-T system with the convolutional coding scheme as illustrated in Figures 12 and 13 and the DVB-T system with the ICI self-cancellation coding scheme as illustrated in Figures 14 and 15.

Both DVB-T systems are benchmarked for three different channel models, namely AWGN, frequency non-selective, and frequency selective channels [11, 21] . We choose the bit-error-rates (BER) versus different signal-to-noise ratios (SNR) to provide

objective quality-of-service comparisons between these two DVB-T systems. The system parameters used in our simulations are described as follows. In our simulations, we choose a QPSK-OFDM-based DVB-T system operating at 2k-mode. The carrier frequency is 600 MHz; the OFDM symbol duration is 298.6667 μsec; the guard interval duration is 1/8 the duration of the OFDM symbol, i.e., 37.333 μsec; the coding rate is 1/2 for both convolutional coder and ICI self-cancellation scheme. Two thousand Monte Carlo trials are simulated and twenty-six OFDM symbols are randomly generated for each trial. The BER curves versus SNR are depicted in Figures 16-25.

Figures 16-18 depict the BER curves for the two DVB-T systems tested for AWGN channels with different normalized frequency offsets $\Delta f_o T$ ($\Delta f_o T$ =0.01, 0.1, 0.2) where Δf_o is the frequency offset which arises from the local oscillator synchronization errors, and T is the OFDM symbol duration [20]. As it can be seen in Figures 16-18, the larger the normalized frequency offsets, the more severe the ICI problem and the worse the DVB-T system performance. According to Figures 16-18, it is noted that the new DVB-T system with the ICI self-cancellation scheme outperforms the existing DVB-T system with the convolutional coding by at least two orders-of-magnitude of BER in a normal SNR condition (SNR=20 dB) for the AWGN channels with different frequency offsets.

In addition, we also tested the two DVB-T systems for the frequency non-selective channels with different Doppler frequency shifts, which are induced by the mobile subscribers at different vehicular speeds.

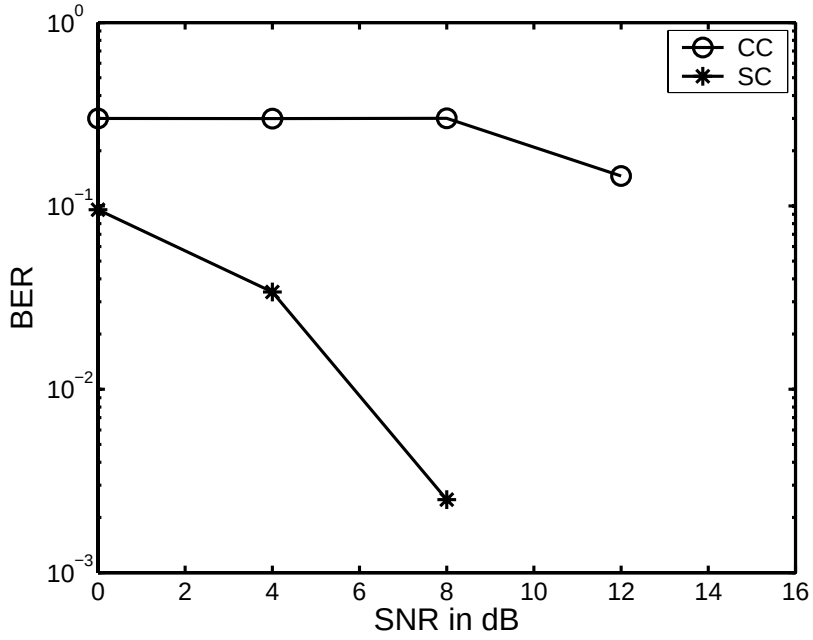

Figure 16. BER comparison between the DVB-T system with ICI self-cancellation scheme (denoted as SC) and the DVB-T system with convolutional coding (denoted as CC) for an AWGN channel with normalized frequency offset $\Delta fT = 0.01$.

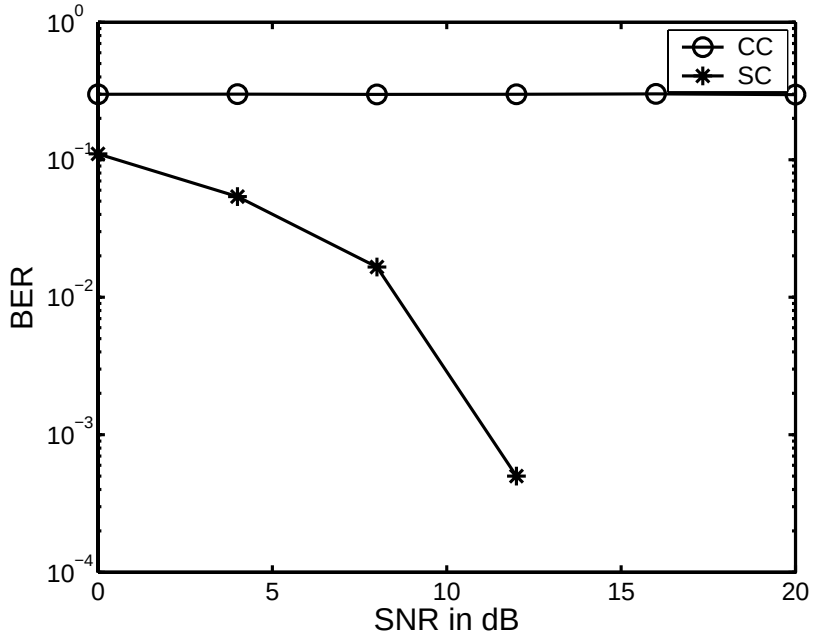

Figure 17. BER comparison between the DVB-T system with ICI self-cancellation scheme (denoted as SC) and the DVB-T system with convolutional coding (denoted as CC) for an AWGN channel with normalized frequency offset $\Delta fT = 0.1$.

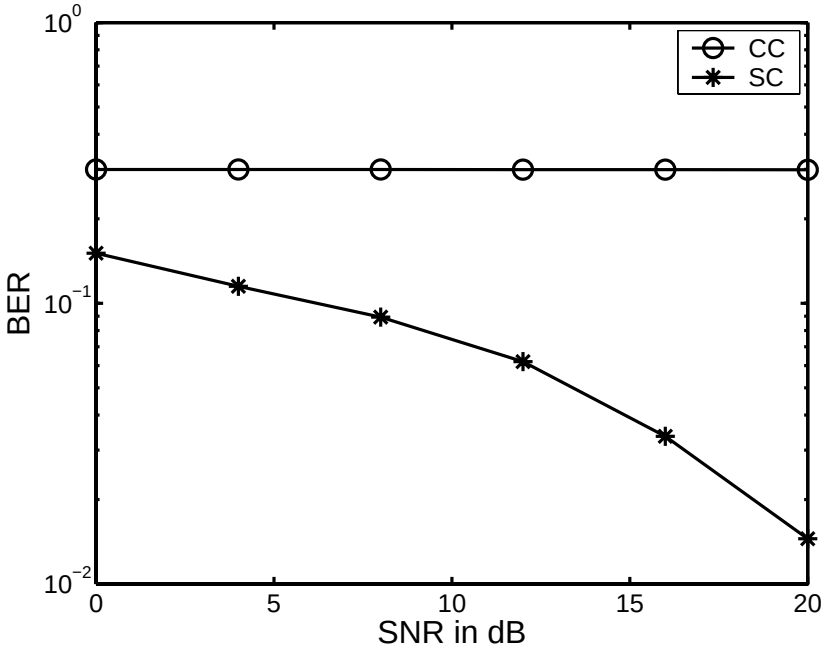

Figure 18. BER comparison between the DVB-T system with ICI self-cancellation scheme (denoted as SC) and the DVB-T system with convolutional coding (denoted as CC) for an AWGN channel with normalized frequency offset $\Delta fT = 0.2$.

Figures19-21 depict the BER curves for the two DVB-T systems tested for these frequency non-selective channels while mobile subscribers are moving at the different speeds (45, 120 and 300 km/h) which give rise to the different equivalent normalized frequency offsets $\Delta f_1 T$ ($\Delta f_1 T = 0.0074, 0.0198, 0.0495$ respectively) [4].

As it can be seen in Figures 19-21, the faster the mobile subscriber moves, the larger the equivalent normalized frequency offset $\Delta f_1 T$, the more severe the ICI problem and the worse the DVB-T system performance. According to Figures 19-21, it is noted that the new DVB-T system with the ICI self-cancellation scheme significantly outperforms the existing DVB-T system with the convolutional coding by many orders-

of-magnitude of BER in a normal SNR condition (SNR=20 dB) for the frequency non-selective channels with different Doppler frequency shifts.

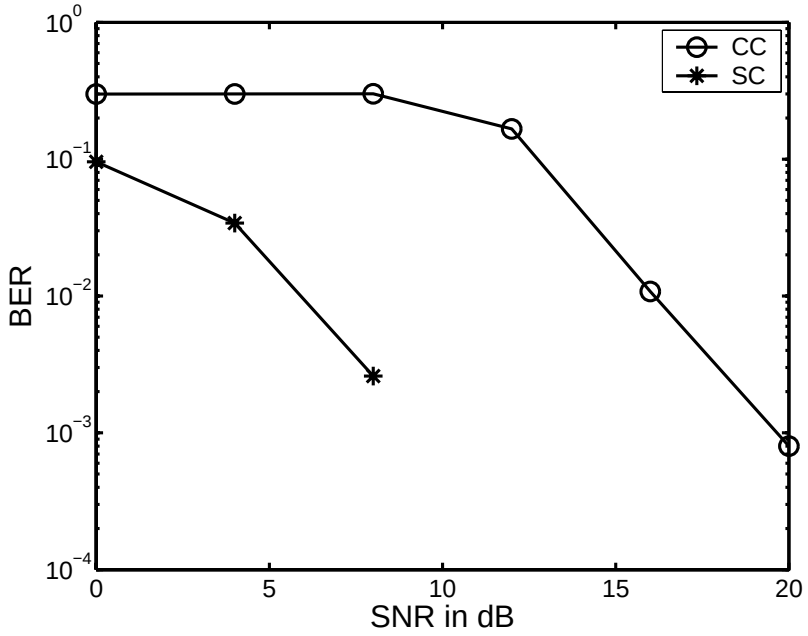

Figure 19. BER comparison between the DVB-T system with ICI self-cancellation scheme (denoted as SC) and the DVB-T system with convolutional coding (denoted as CC) for a frequency non-selective channel with the Doppler frequency shift induced by a mobile subscriber at the speed of 45 km/h (equivalent normalized frequency offset $\Delta fT = 0.0074$).

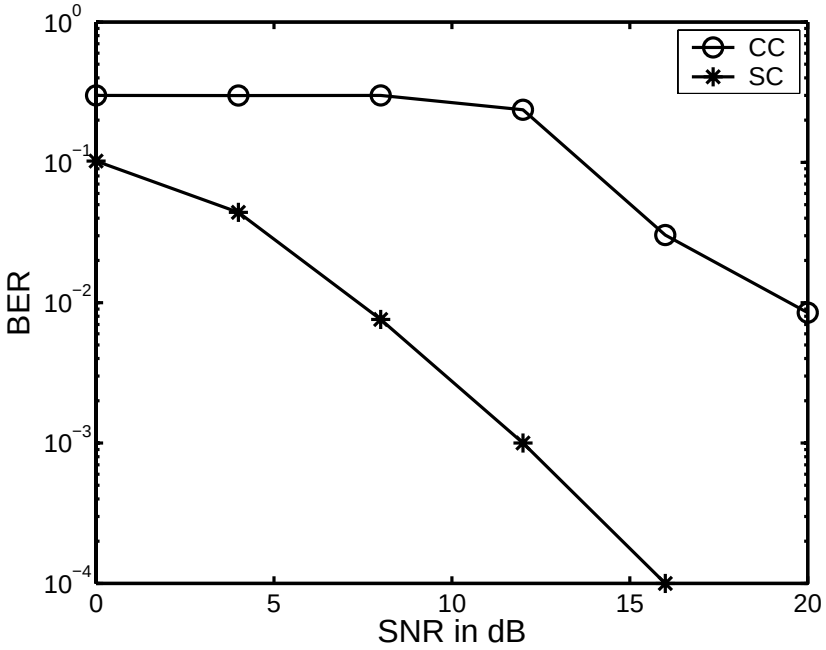

Figure 20. BER comparison between the DVB-T system with ICI self-cancellation scheme (denoted as SC) and the DVB-T system with convolutional coding (denoted as CC) for a frequency non-selective channel with the Doppler frequency shift induced by a mobile subscriber at the speed of 120 km/h (equivalent normalized frequency offset $\Delta fT = 0.0198$).

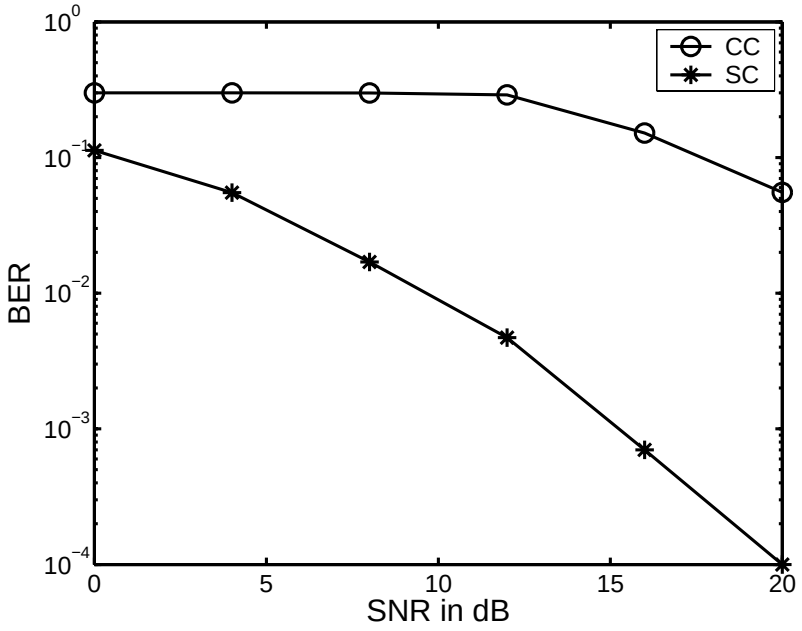

Figure 21. BER comparison between the DVB-T system with ICI self-cancellation scheme (denoted as SC) and the DVB-T system with convolutional coding (denoted as CC) for a frequency non-selective channel with the Doppler frequency shift induced by a mobile subscriber at the speed of 300 km/h (equivalent normalized frequency offset $\Delta fT = 0.0495$).

Finally, we would like to provide another set of simulation results for the frequency selective fading channels. The channels we adopt are the COST 207 channels for rural (non-hilly), urban (non-hilly), hilly urban, and hilly terrain areas [31]. Figures 22-25 depict the BER curves for the two DVB-T systems tested for these frequency selective channels according to the COST 207 model. According to Figures 22-25, the DVB-T system performances are seriously degraded due to these frequency selective fadings. However, the two DVB-T systems either with ICI self-cancellation scheme or with convolutional coding provide the same level of quality-of-service in terms of the BER.

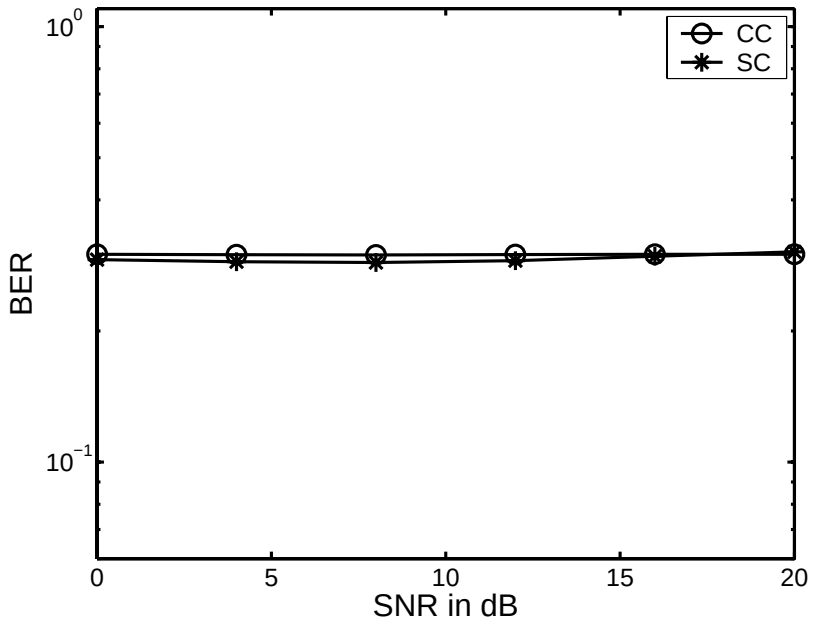

Figure 22. BER comparison between the DVB-T system with ICI self-cancellation scheme (denoted as SC) and the DVB-T system with convolutional coding (denoted as CC) in a frequency selective channel for non-hilly rural areas.

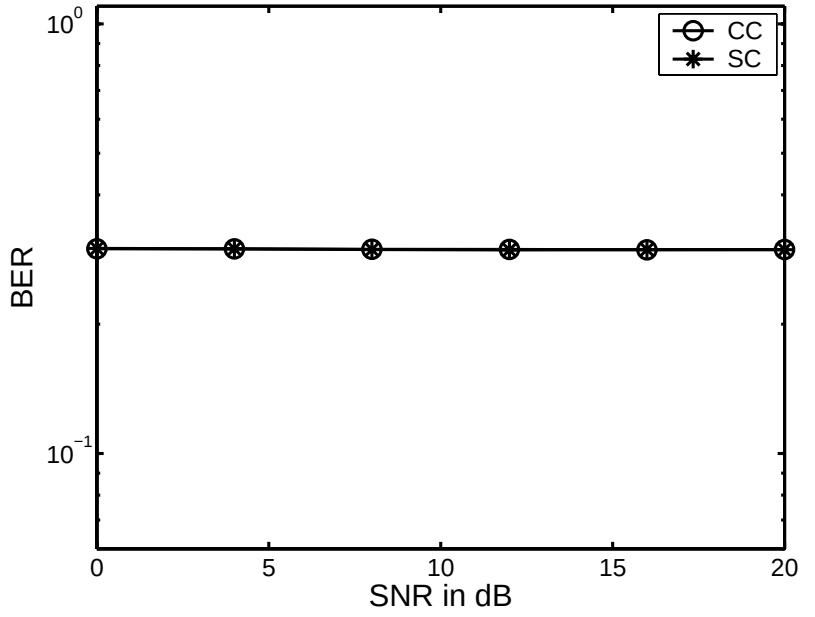

Figure 23. BER comparison between the DVB-T system with ICI self-cancellation scheme (denoted as SC) and the DVB-T system with convolutional coding (denoted as CC) in a frequency selective channel for non-hilly urban areas.

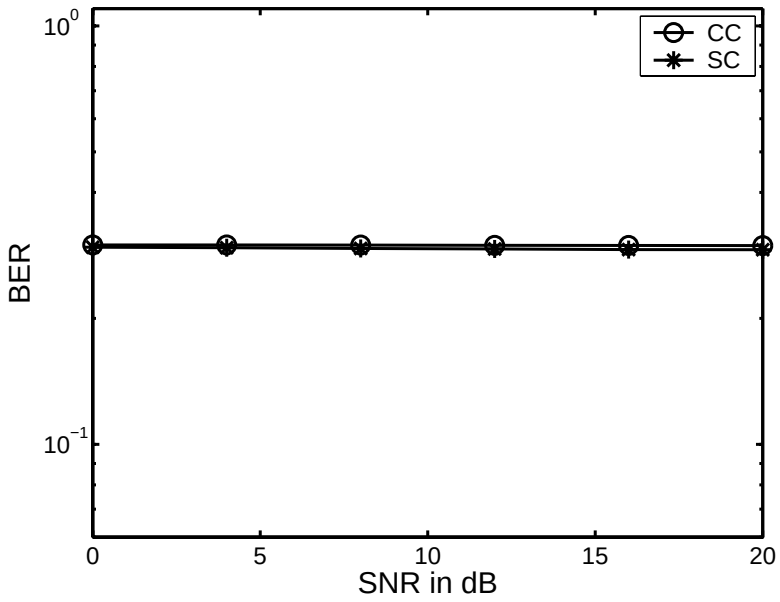

Figure 24. BER comparison between the DVB-T system with ICI self-cancellation scheme (denoted as SC) and the DVB-T system with convolutional coding (denoted as CC) in a frequency selective channel for hilly urban areas.

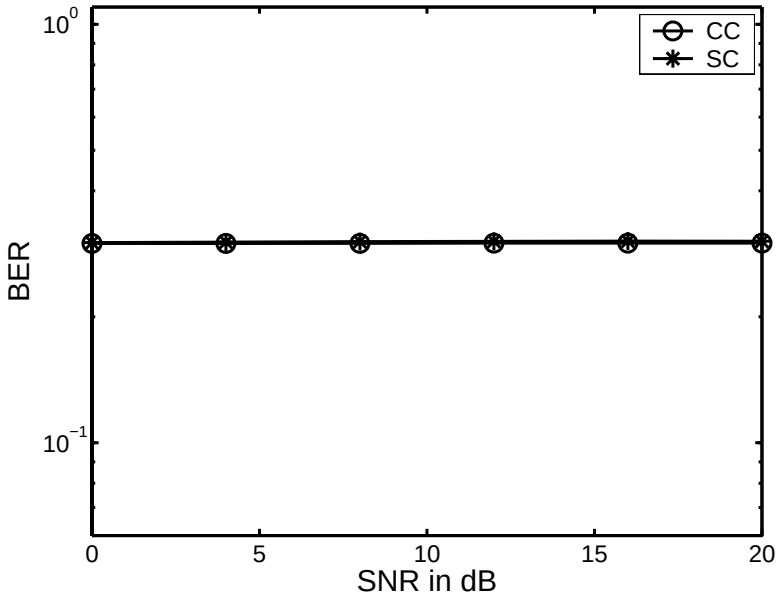

Figure 25. BER comparison between the DVB-T system with ICI self-cancellation scheme (denoted as SC) and the DVB-T system with convolutional coding (denoted as CC) in a frequency selective channel for hilly terrain areas.

CHAPTER 5
CONCLUSION

In this thesis, we establish a simulation tool for the digital video broadcasting (DVB-T) systems. Besides, since the current DVB systems are based on orthogonal frequency division multiplexing (OFDM), we study the OFDM system and identify the corresponding crucial problem, namely intercarrier interference (ICI). In addition, we present the fading channel models for the digital video broadcasting, namely additive white Gaussian noise (AWGN), frequency non-selective and frequency selective channels.

Meanwhile, we extend one of the effective ICI-mitigation schemes, the ICI self-cancellation method which was introduced for the plain OFDM systems, to have a full investigation on the DVB-T system for the aforementioned different fading channels. We compare the new DVB-T system with this ICI self-cancellation scheme to the current DVB-T system with the convolutional coding through our simulation tool.

In summary, the DVB-T system with the ICI self-cancellation scheme significantly outperforms the existing DVB-T system with the convolutional coding in terms of BER for several orders-of-magnitude when they operate in the AWGN and the frequency non-selective channels with a normal signal-to-noise ratio condition (SNR=20 dB). However, both DVB-T systems perform similarly in the frequency selective channels according to the COST 207 model.

REFERENCES

[1] U. Reimers, "Digital video broadcasting," *IEEE Communications Magazine,* vol. 36, no. 6, pp.104 – 110, June 1998.

[2] M. Kornfeld, "DVB-H – The emerging standard for mobile data communication," *IEEE International Symposium on Consumer Electronics*, pp. 193-198, September 2004.

[3] G. Proakis, *Digital Communications*, 4th Edition., McGraw-Hill, 2001.

[4] T. S. Rappaport, *Wireless Communications Principles and Practice*, Prentice-Hall, 1996.

[5] ETSI, "Digital broadcasting systems for television, sound and data services; framing structure, channel coding and modulation for 11/12 GHz satellite services," ETSI ETS 300 429 December 1994.

[6] ETSI, "Digital broadcasting systems for television, sound and data services; framing structure, channel coding and modulation for cable systems," ETSI ETS 300 421 December 1994.

[7] F. Kuchen, D.L. Didascalou and W. Wiesbeck, "Terrestrial network planning for digital video broadcasting to mobile receivers," *IEEE Vehicular Technology Conference*, vol. 3, pp.1889-1893, May 1998.

[8] R. Burow, K. Fazel, P. Hoeher, O. Klank, H. Kussmann, P. Pogrzeba, P. Robertson and M. J. Ruf, "On the performance of the DVB-T system in mobile environment," *Proceedings of IEEE Global Telecommunications Conference*, vol. 4, pp. 2198-2204, November 1998.

[9] I. Gaspard, "Mobile reception of the terrestrial DVB-system," *IEEE Vehicular Technology Conference*, vol. 1, pp. 151-155, May 1999.

[10] A.M. Gallardo, M.E. Woodward and J. Rodriguez-Tellez, "Performance of DVB-T OFDM based single frequency networks: effects of frame synchronisation, carrier frequency offset and non-synchronised sampling errors," *IEEE Vehicular Technology Conference*, vol. 2, pp. 962-966, October 2001.

[11] J. Rinne, "Some elementary suboptimal diversity reception schemes for DVB-T in mobile conditions," *IEEE Transactions on Consumer Electronics*, vol. 46, no. 3, pp. 847-850, August 2000 .

[12] ETSI EN 300 744 V1.4.1 (2001-01): “Digital video broadcasting (DVB); framing structure, channel coding and modulation for digital terrestrial television,” ETSI, 2001.

[13] J. S. Choi, J. W. Kim, D. S. Han, J. Y. Nam, Y. H. Ha, “Design and implementation of DVB-T receiver system for digital TV,” *IEEE Transaction on Consumer Electronics*, vol. 50, no. 4, pp. 991-998, November 2004.

[14] J. Vare and M. Puputti, “Soft handover in terrestrial broadcast networks,” *IEEE International Conference on Mobile Data Management* pp. 236-242, 2004.

[15] J. Vare, A. Hamara and J. Kallio, “Approach for improving receiver performance in loss-free handovers in DVB-H networks,” *Proceedings of IEEE Global Telecommunications Conference* 2004, v 5, pp. 3326-3331.

[16] B. Sklar, “Rayleigh fading channels in mobile digital communication systems, part 1: characterization,” *IEEE Communication Magazine*, vol. 35, no. 7, pp. 102-109, July 1997.

[17] H.-C. Wu and X. Huang, "Joint phase/amplitude estimation and symbol detection for wireless ICI self-cancellation coded OFDM systems," *IEEE Transactions on Broadcasting*, vol. 50, no. 1, pp. 49-55, March 2004.

[18] M.Speth, S.A.Fechtel, G.Fock and H.Meyr, "Optimum receiver design for wireless broad-band systems using OFDM - part I," *IEEE Transactions on Communications*, vol. 47, no. 11, pp. 1668 - 1677, November 1999.

[19] B. Sklar, “Rayleigh fading channels in mobile digital communication systems, part 2: mitigation,” *IEEE Communication Magazine*, vol. 35, no. 7, pp. 90-100, July 1997.

[20] J. Armstrong, “Analysis of new and existing methods of reducing intercarrier interference due to carrier frequency offset in OFDM,” *IEEE Transactions on Communications*, vol. 47, no. 3, pp. 365-369, March 1999.

[21] M. Torabi, M.R. Soleymani, “COFDM with orthogonal transmit diversity and power control for broadband wireless communications,” *Canadian Conference on Electrical and Computer Engineering*, vol. 3, pp. 1331-1336, May 2002.

[22] T. Pollet, M. V. Bladel and M. Moeneclaey, “BER sensitivity of OFDM systems to carrier frequency offset and Wiener phase noise,” *IEEE Transactions on Communications*, vol. 43, no. 2-4 pt 1, pp. 191-193, February-April 1995.

[23] P. H. Moose. “Technique for orthogonal frequency division multiplexing frequency offset correction,” *IEEE Transactions on Communications*, vol. 42, no. 10, pp. 2908-2914, October 1994.

[24] H.-C. Wu and G. Gu, "Analysis of intercarrier and interblock interferences in wireless OFDM systems," *Proceedings of IEEE Global Telecommunications Conference*, vol. 2, pp. 784-788, December 2003.

[25] M. Gudmundson and P.-O. Anderseon, "Adjacent channel interference in an OFDM system," *IEEE Vehicular Technology Conference*, vol. 2, pp. 918-922, 1996.

[26] C. Muschallik, "Improving an OFDM reception using an adaptive Nyquist windowing," *IEEE Transactions on Consumer Electronics*, vol. 42, no. 3, pp. 259-260, August 1996.

[27] Y. Zhao and S.-G. Haggman, "Intercarrier interference self-cancellation scheme for OFDM mobile communication systems," *IEEE Transactions on Communications*, vol. 49, no. 7, pp. 1185-1191, July 2001.

[28] M. Kornfeld and U. Reimers, "DVB-H - The emerging standard for mobile data communication," *EBU Technical Review*, no. 301, January 2005.

[29] C.-T. Chen, *Signals and Systems*, 3rd Edition, Oxford University Press, 2004.

[30] J. Armstrong, P.M. Grant and G. Povey, "Polynomial cancellation coding of OFDM to reduce intercarrier interference due to Doppler spread," *Proceedings of IEEE Global Telecommunications Conferenc*e, vol. 5, pp. 2771-2776, November 1998.

[31] A. F. Molisch, *Wideband wireless digital communications*, Prentice-Hall, 2001.

VITA

Khaled Matarneh was born in Jordan on October 10th, 1981. He grew up in Amman, Jordan, till he was 17, that's when he traveled to the United States to pursue his college education. He was awarded a scholarship in 1999 to go to the University of Arkansas in Fayetteville for his bachelor degree of science in electrical engineering where he graduated with honors in 4 years. After graduating from University of Arkansas, he decided to pursue his master's degree of science in electrical engineering at Louisiana State University in Baton Rouge.